



To seal or not to seal: The closure dynamics of a splash curtainJavad Eshraghi ¹, Sunghwan Jung ², and Pavlos P. Vlachos ^{1,*}¹*Department of Mechanical Engineering, Purdue University, West Lafayette, Indiana 47907, USA*²*Department of Biological and Environmental Engineering, Cornell University, Ithaca, New York 14853, USA*(Received 15 December 2019; accepted 11 September 2020;
published 1 October 2020)

When an object impacts the free surface of a liquid, it ejects a splash curtain upwards and creates an air cavity below the free surface. As the object descends into the liquid, the air cavity eventually closes under the action of hydrostatic pressure (deep seal). In contrast, the surface curtain may splash outwards or dome over and close, creating a surface seal. In this paper, we experimentally investigate how the splash curtain dynamics are governed by cavity pressure difference, gravity, and surface tension, and how their interplay controls the occurrence, or not, of the surface seal. Based on the experimental observations and measurements, we develop an analytical model to describe the trajectory and dynamics of the splash curtain. The model enables us to reveal the scaling relationship for the dimensionless surface seal time and discover the existence of a critical dimensionless number that predicts the occurrence of the surface seal. This scaling indicates that the most significant parameter governing the occurrence of a surface seal is the velocity of the airflow rushing into the cavity, which is in contrast to the current understanding that considers the impact velocity as the determinant parameter.

DOI: [10.1103/PhysRevFluids.5.104001](https://doi.org/10.1103/PhysRevFluids.5.104001)**I. INTRODUCTION**

Splashes are ubiquitous in nature and engineering as a result of an object's impact on a free surface (known as water entry) and govern processes from diving to ocean oxygenation. Work on water entry has been predominantly focused on the dynamics and fluid motion that occur below the surface [1–7], often not considering the dynamics of the splash curtain [2,8].

The study of splashes is dating back to 1908, where Worthington [9] published the results of his photographic investigations on crowns. Since then, two forces have been postulated as the driving factors for the closure of splashes: the cavity pressure difference with respect to the ambient, caused by the airflow rushing into the cavity behind the sphere, and the surface tension [10]. However, the interplay of these forces has been controversial, and some works selectively neglect one of the two and focus on the other as the governing parameter of the surface seal, in order to explain the closure of the splash curtain.

Gilbarg and Anderson [10] examined the splash evolution and closure under reduced pressure and assumed that the pressure drop across the splash curtain was equal to the dynamic pressure term from the Bernoulli equation, $1/2\rho V_0^2$, where ρ is air density and V_0 is the speed of the sphere at impact. In another study, Yakimov [11], who was investigating the effects of ambient pressure on the splash curtain, attributed the surface seal to the higher air drag experienced by the tip of the splash (referred to as rounded rim in our paper), which is responsible for the accumulation of liquid at the tip and relative thickening in comparison with splashes at lower ambient pressures. Furthermore, he

*pvlachos@purdue.edu

estimated the pressure drop across the splash as $\Delta P = 1/2\rho(V_0^2 + 2V_0V_1)$, where V_0 is the airflow velocity, assumed to be the same as the projectile impact velocity, and V_1 is the velocity of the tip of the splash curtain ejecting upwards and outwards from the impact location. However, Abelson [12] and Lee *et al.* [13] showed that the Bernoulli pressure drop is an underestimation of the actual pressure difference.

In addition to the studies that considered the pressure difference as the most significant factor in the surface seal, investigations of the interplay between inertia and surface tension at the length scale of the splash curtain thickness suggest that surface tension plays a significant role. Marston *et al.* [14] investigated splashes formed for different surface tension values and concluded that surface tension is not negligible in the surface sealing phenomena. Aristoff and Bush [15] presented an analysis of the water entry of small hydrophobic spheres, which also proposed a phenomenological model of the splash curtain shape at the time when it was assumed that the pressure differential was negligible, thus suggesting that the splash closure was primarily driven by surface tension. Also, these studies did not introduce any criteria for the transition from no surface-seal regime to surface-seal regime.

Hence, understanding what controls the occurrence of the surface seal during water entry remains elusive. As such, the principal aim of this study is to elucidate the role of the forces acting on the splash curtain and derive the physical mechanism that governs the surface seal. In doing so, we present detailed analysis and explanations of the splash curtain dynamics, supported by a physical model and experimental observations, and show that the pressure difference is not negligible, and provide a scaling parameter that predicts the occurrence of the surface seal.

II. EXPERIMENTAL PROCEDURE

To study the dynamics of the splash curtain, we drop different spheres into a $25 \times 40 \times 50\text{-cm}^3$ glass-sided aquarium tank filled with distilled water and record the phenomena using a high-speed digital video camera operating at 5000 fps. The tank does not interfere with cavity expansion or pinch-off for any of the experiments reported. The dropping mechanism is mounted above the tank to release spheres without imparting spin, which can strongly affect the cavity dynamics [7].

The projectiles used here include acrylic ($\rho_s = 1.18 \text{ g/cm}^3$), glass ($\rho_s = 2.40 \text{ g/cm}^3$), alumina ($\rho_s = 3.96 \text{ g/cm}^3$), steel ($\rho_s = 7.87 \text{ g/cm}^3$), and tungsten ($\rho_s = 19.30 \text{ g/cm}^3$) spheres of different diameters ($d = 9.525\text{--}19.05 \text{ mm}$). In order to produce a cavity, the projectiles are coated with WX2100 [9,16], which creates a hydrophobic surface condition with a contact angle of $150^\circ\text{--}165^\circ$. The sphere impact velocities ranged from 2.0 to 6.0 m/s (by 0.5-m/s increments). The impact of a projectile of radius R_0 into a liquid at velocity U_0 is characterized by the nondimensional Froude number $Fr = U_0/\sqrt{gR_0}$, where g is the gravitational acceleration [17,18]. The Reynolds number (Re), the Weber number (We), and the Bond number (Bo) are also often used to provide insight into the interplay and relative importance of the physical forces governing free-surface interaction in the water-entry phenomenon; $Re = R_0U_0/\nu$ where ν is the kinematic viscosity of the liquid, $We = \rho U^2 R_0/\gamma$ where ρ is the liquid density and γ is the surface tension, $Bo = \Delta\rho g R_0^2/\gamma$ where $\Delta\rho$ is the density difference.

III. EXPERIMENTAL OBSERVATIONS

During the initial stages of impact, a splash curtain is ejected upwards and outwards, as seen in Fig. 1 [19]. In addition, as the sphere descends into the fluid, an expanding air cavity is formed behind it [20].

As the splash rises from the surface, it is subject to two main forces leading to its collapse: reduction in pressure caused by the airflow entrained into the cavity behind the sphere, and surface tension [13,21]. The air flowing into the expanding cavity induces pressure drag acting on the splash curtain and draws the splash radially inward. Surface closure is critical in the development of the cavity and influences the later cavity growth [16,22]. After surface closure, the cavity continues to

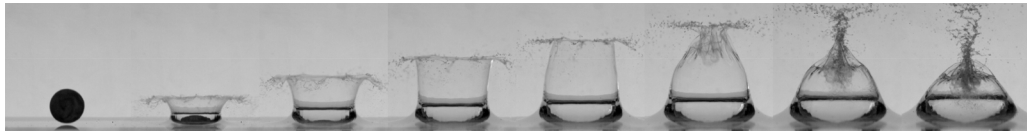


FIG. 1. Splash curtain formed by a steel sphere, $R_0 = 0.95$ cm, $U_0 = 5.5$ m/s, $\Delta t = 3$ ms.

expand due to the inertial effects of the sphere moving through the fluid, and the pressure inside the cavity decreases. The pressure governing the deep seal in the impact-produced cavities is the sum of the hydrostatic pressure due to the depth [13,17] and the pressure deficit in the cavity [21,23]. The higher the pressure difference between cavity and air above the surface, the closer the pinch-off location will be to the surface [10,23].

Our observations show that the cavity characteristics are highly dependent on the sphere density and do not scale linearly with Fr as had been observed experimentally by Ref. [24] for low Fr ; the deviation is most pronounced for the cases with surface seal. Even though the modified expressions for cavity characteristics developed by Ref. [8] agree with experimental observations in the regime without surface seal, they are not reliable in the surface-seal regime, since the effect of surface seal on the cavity is ignored [25].

In the closure of the splash curtain, an intuitive interpretation might label an impact velocity as the primary cause in the occurrence of surface-seal phenomenon. However, experimental observations imply dependency of the surface seal not only on the sphere impact velocity but also on the sphere size and density. To identify the surface closure mechanism, we will look at the interactions between the forces acting on the splash curtain, pulling it inward.

IV. SPLASH CURTAIN MODELING

Shortly after the splash is ejected upon impact, surface tension causes the fluid at the tip of the splash to coalesce, forming a rounded rim. This rim is approximated as an axisymmetric circular ring about the z axis, attached to a thin fluid film. In reality, the splash is very irregular, often forming a crownlike splash similar to those observed by Refs. [14,26].

The vector $\vec{x}(t) = r(t)\hat{r} + z(t)\hat{z}$, describes the position of the rim in the r - z plane. Figure 2(a) shows the splash geometry and coordinate system just after the impact. Normal, \hat{n} , and tangential, \hat{s} , coordinates are also defined relative to the rim, in the direction of its instantaneous velocity. The angle θ is defined as the angle from the \hat{r} unit vector to the \hat{s} unit vector. Figure 2(b) shows the splash curtain at some later time as the trajectory of the splash has evolved. As the rim's trajectory evolves, the \hat{n} and \hat{s} coordinates remain fixed to the rim, and their orientation is described by the angle θ .

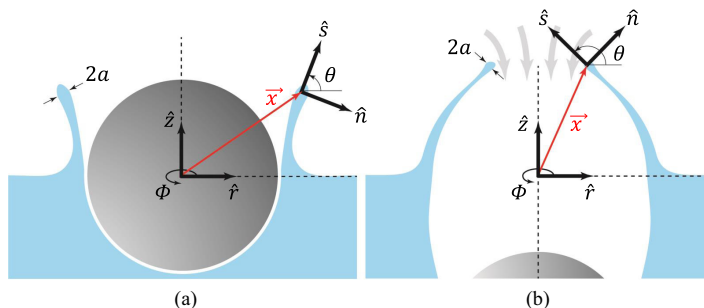


FIG. 2. The coordinate system: (a) right after impact, (b) right before the surface seal.

The rounded rim is approximated by a finite mass, constant in time, with a circular profile in the r - z plane. The rim radius, a , is obtained from the experiment and assumed to be constant in time. With the assumed geometry and the coordinate system shown in Fig. 2, a differential volume of the rim is given by $\rho\pi a^2 r d\phi$. This small mass is moving in a curved trajectory and has a centrifugal acceleration. This acceleration creates a force given by

$$\vec{F}_c(t) = \rho\pi a^2 r(t) d\phi \frac{|\dot{\vec{x}}(t)|^2}{R_c(t)} \hat{n}, \quad (1)$$

where $R_c(t)$ is the instantaneous radius of curvature of the rim's trajectory given by

$$R_c(t) = \frac{d\theta(t)}{ds}. \quad (2)$$

A drag force opposes the rim's motion, as the ejected fluid travels through the surrounding air. The drag force is given by

$$\vec{F}_d(t) = -\frac{1}{2}\rho_a C_d 2ar(t) d\phi |\dot{\vec{x}}(t)|^2 \hat{s}, \quad (3)$$

where C_d is the drag coefficient. There have been many attempts to model the drag coefficient on drops and thin liquid sheets [27]. For simplicity, we have chosen to approximate the airflow around the rounded rim to be laminar, and the drag coefficient may be expressed as $C_d = 24/Re$.

Two surface-tension forces need to be considered [28,29]. The first is a result of the thin fluid sheet attached to the rounded rim, given by

$$\vec{F}_{\gamma 1}(t) = -2\gamma r(t) d\phi \hat{s}. \quad (4)$$

The sheet pulls the rim along the s direction, and we must account for both sides of the thin film (thus the factor of 2). The second surface-tension force acts along the circumference of the rim, radially inward, given by

$$\vec{F}_{\gamma 2}(t) = -4\pi a\gamma d\phi \hat{r}. \quad (5)$$

There is a gravitational force acting in the z direction [28,29], given by

$$\vec{F}_g(t) = -\rho g\pi a^2 r(t) d\phi \hat{z}. \quad (6)$$

The expanding air cavity creates a pressure difference across the splash curtain. This pressure difference acts normal to the splash trajectory, collapsing it inward. This pressure difference creates a force given by

$$\vec{F}_{\Delta P}(t) = -2ar(t) d\phi \Delta P(t) \hat{n}, \quad (7)$$

where $\Delta P(t)$ is the pressure difference across the splash. This pressure difference can be estimated by measuring the time rate of change of cavity volume, $dV_{cav}(t)/dt$. If the cavity is treated as a control volume, the rate of expansion (or collapse) can be thought of as the volumetric flow rate of air from the surrounding atmosphere into the cavity. If the area of the opening through which airflow is known, a mean air velocity, $U_{air}(t)$, can be estimated. With this mean air velocity, a pressure drop can be estimated using Bernoulli's principle.

The cavity was assumed to be axisymmetric about the z axis [Fig. 3(a)]. Integrating the cavity radius, $R(z, t)$, over the length of the cavity, $Z(t)$, at each time step yields the cavity volume history. An image-processing routine was developed to determine the cavity profile from the captured image data and calculate the cavity volume, $V_{cav}(t)$.

As the sphere travels downward, it opens up and expands the air cavity behind it. As the cavity expands, air is drawn into the cavity from the surrounding atmosphere. Neglecting compressibility effects, the time rate of change of cavity volume describes the volumetric flow rate of air into the cavity, given by

$$Q(t) = \frac{dV_{cav}(t)}{dt}, \quad (8)$$

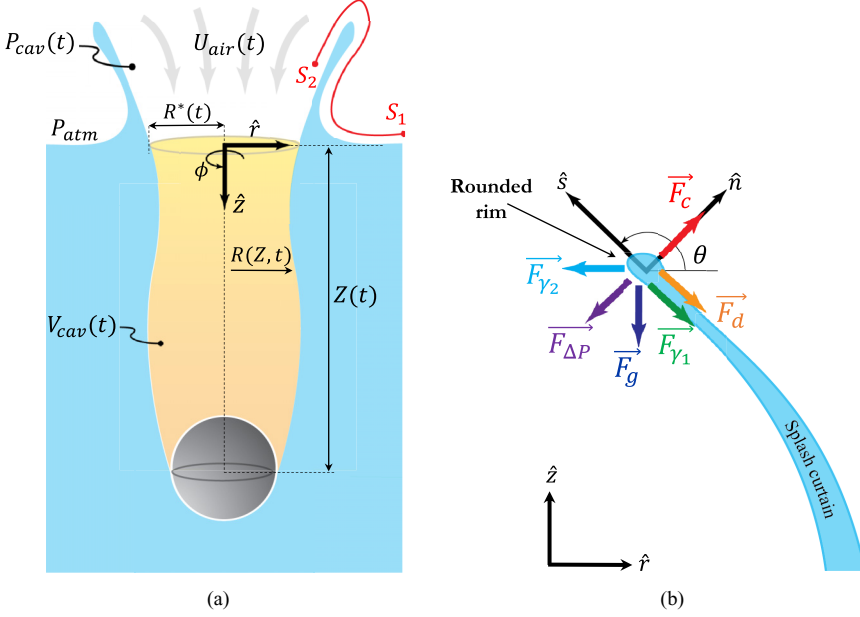


FIG. 3. (a) Cavity behind the sphere. The cavity volume, $V_{cav}(t)$, can be approximated by integrating the cavity profile, $R(z, t)$, over the length of the cavity, $Z(t)$. (b) Forces acting on the rounded rim of the splash curtain.

where $Q(t)$ is the volumetric flow rate. In order to suppress the amplification of noise, which can often be a problem for numerical derivatives, the cavity volume data were lightly smoothed using robust, locally weighted regression [30]. After the smoothing, a fourth-order central difference scheme was used to compute the derivative [31].

If the area of the opening through which the air flows is known, a mean air velocity, $U_{air}(t)$, can be estimated. We already found the cavity profile for cavity volume determination; thus, we consider the opening radius, R^* , at each time instant, t_i , as the $R^*(t = t_i) = R(z = 0, t_i)$, and the cavity opening area is $\approx \pi R^{*2}$. Hence, the mean airflow velocity can be estimated by

$$U_{air}(t) \approx \frac{Q(t)}{\pi R^{*2}}. \quad (9)$$

This provides an estimate of the mean air velocity flowing from the surrounding atmosphere, past the splash curtain, into the air cavity. We can use this condition to estimate a cavity pressure using Bernoulli's principle. Picking two arbitrary points along a streamline, one outside the cavity and the other inside the cavity, we can write

$$\left[\rho gz + \frac{1}{2} \rho U^2 + P \right]_{S_1} = \left[\rho gz + \frac{1}{2} \rho U^2 + P \right]_{S_2}, \quad (10)$$

where S_1 is some position far away from the cavity and S_2 is a position just inside the cavity, close to the rounded rim, as seen in Fig. 3(a). Position S_1 was assumed to be at atmospheric pressure with no air motion. Position S_2 was assumed to be at cavity pressure, $P_{cav}(t)$, and have an airflow velocity of $U_{air}(t)$, given by Eq. (9). Neglecting changes in elevation and assuming cavity conditions are constant throughout the cavity (not varying in space), the pressure difference across the splash can be estimated by

$$\Delta P(t) = P_{atm} - P_{cav}(t) = \frac{1}{2} \rho U_{air}^2(t), \quad (11)$$

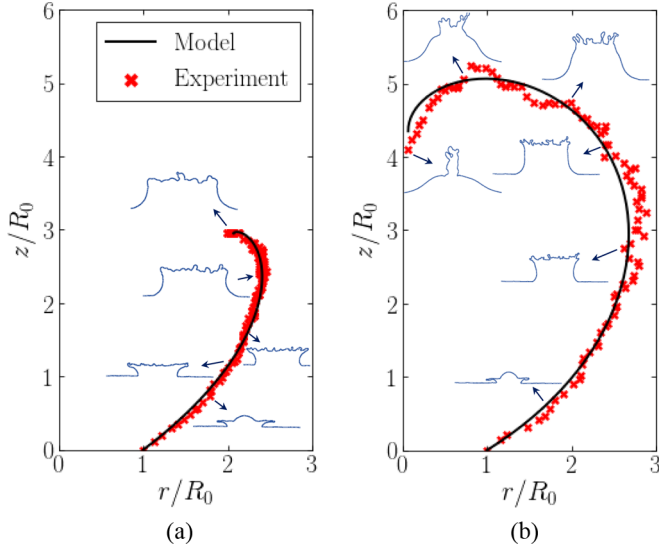


FIG. 4. Splash curtain rounded rim trajectory: Experimental observation vs model prediction. (a) $We \approx 800$, $Bo \approx 12$, $DR = 7.87$, $U_{air,m}/U_0 \approx 0.1063$, (b) $We \approx 3950$, $Bo \approx 12$, $DR = 7.87$, $U_{air,m}/U_0 \approx 0.9474$ [32]. Density ratio: $DR = \rho_s/\rho$, where ρ_s is sphere density.

where $\Delta P(t)$ is the pressure difference across the splash. This assumes the air flowing into the cavity is incompressible, viscous effects are negligible, and treats the cavity as a spatially uniform body. We will also assume that $P(t)$ is spatially uniform within the cavity. Figure 2(b) shows these forces and their directions relative to the splash curtain.

In this model, the force from the liquid sheet is ignored due to difficulty in measurement and estimation of fluid flow inside the thin sheet. Without experimental measurements, to estimate this force, we need to introduce several unknowns in the model, which will make the model complicated and more like a simple fitting. So, since the splash thickness is small, it is safe to ignore this effect.

Summing these forces results in an equation of motion for the rim, given by

$$\rho\pi a^2 r(t) d\phi \frac{d^2 \vec{x}(t)}{dt^2} = \vec{F}_c + \vec{F}_{\gamma 1} + \vec{F}_{\gamma 2} + \vec{F}_g + \vec{F}_d + \vec{F}_{\Delta P}. \quad (12)$$

Simplifying Eq. (12) results in a second-order nonlinear ordinary differential equation describing the motion of the splash rim. The splash originates at a radial distance R_0 at the free surface ($z = 0$). The initial conditions in space are given by $\vec{x}(t = 0) = R_0 \hat{r}$. The initial conditions for velocity are given by $\dot{\vec{x}}(t = 0)$, which is obtained from the experiment.

For a chosen set of system parameters and initial conditions, the trajectory of the splash curtain can be modeled by solving Eq. (12). To validate the proposed model, we compare the rim trajectory predicted by the model with experimental observations in Fig. 4 [32,33]. We define the first inflection point found in the splash curtain profile from the bottom of the curtain as the curtain rounded rim in the experimental videos (see Appendix 1).

Surface seal occurs when $r(t) = 0$. At this moment, the rounded rim has only one velocity component in the negative \hat{z} direction. Thus, the occurrence of a surface seal is defined by two criteria given by

$$t_{\text{surf}} \rightarrow \dot{r}(t) = 0 \text{ and } \dot{z}(t) < 0, \quad (13)$$

where t_{surf} is the time elapsed between the initial impact of the sphere and the surface seal. The model predicts the surface seal as when the two criteria in Eq. (13) are met. In the cases without surface seal, the time it takes for the splash to reach its maximum height is considered as the

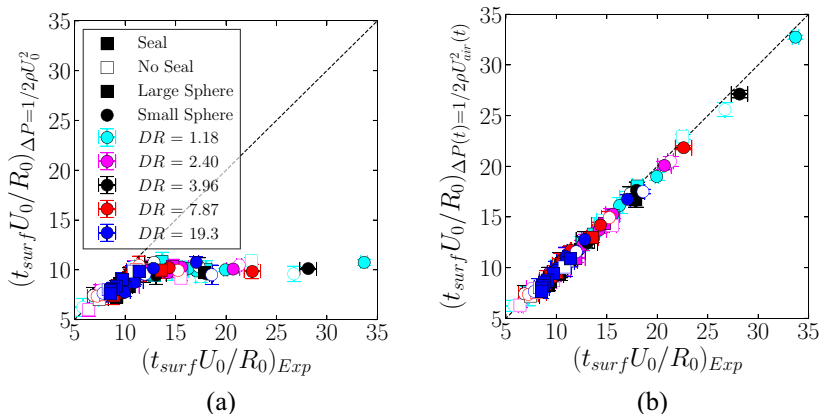


FIG. 5. Model prediction for dimensionless surface-seal time vs measured value for two different approaches in pressure difference estimation. In (a), pressure difference was defined based on the sphere impact velocity, while in (b) the pressure difference was estimated using the cavity volume method. Cases without surface seal are shown with open markers.

equivalent seal time, and the same criteria [Eq. (13)] are applied for modeling of these cases as well.

V. DISCUSSION

The results of the model are susceptible to the pressure force. In the establishment of the pressure difference, we used the airflow velocity. Another approach for the formulation would be replacing the airflow velocity with the sphere impact velocity. Figure 5 shows a comparison between the surface-seal time predicted by the model and the measured value from the experiment as well as the model performance sensitivity to the velocity selection in pressure difference formulation. Figure 5(a) indicates that the surface-seal time predicted by the constant pressure difference, defined based on the sphere impact velocity, does not agree with the experimental measurements. On the other hand, by taking into account the instantaneous pressure difference across the splash curtain [Fig. 5(b)], which is a representation of the cavity expansion history and airflow velocity, the maximum model error in the prediction of surface-seal time is 5.6%.

Also, we report the dimensionless surface-seal time as a function of We , defined based on sphere impact velocity, in Fig. 6(a). Despite showing the general decaying trend with We , this scaling fails to identify a critical We for the transition from no surface-seal regime to surface-seal regime for all the spheres with different density and size [34].

Aristoff and Bush [15] scaled the dimensionless surface-seal time with We and claimed that for $Bo \leq 3$ the surface seal occurs when the We exceeds ≈ 300 . However, our observations show that this value has been underestimated, and how this value depends on the sphere density remained unexplored. For all the conditions tested, this surface-seal criterion did not predict correctly the transition from no surface-seal regime to surface-seal regime and we observed no surface seal for $We < 850$ for the spheres with $Bo \approx 3$. Another proposed scaling for the surface-seal time is based on the sphere impact velocity [10,13,23] which also has the same limitation as We scaling. Namely, the impact velocity beyond which the surface seal occurs depends on sphere density and size. This limitation resulted in Refs. [10,13,23] not proposing any criterion for the occurrence of surface seal based on the sphere impact velocity.

These observations indicate that the sphere impact velocity is not the most significant parameter in the surface closure process. Based on the experiment, water-entry cavities with quickly increasing volumes [high $dV_{cav}(t)/dt$ values] are associated with surface seal. In other words, surface-seal

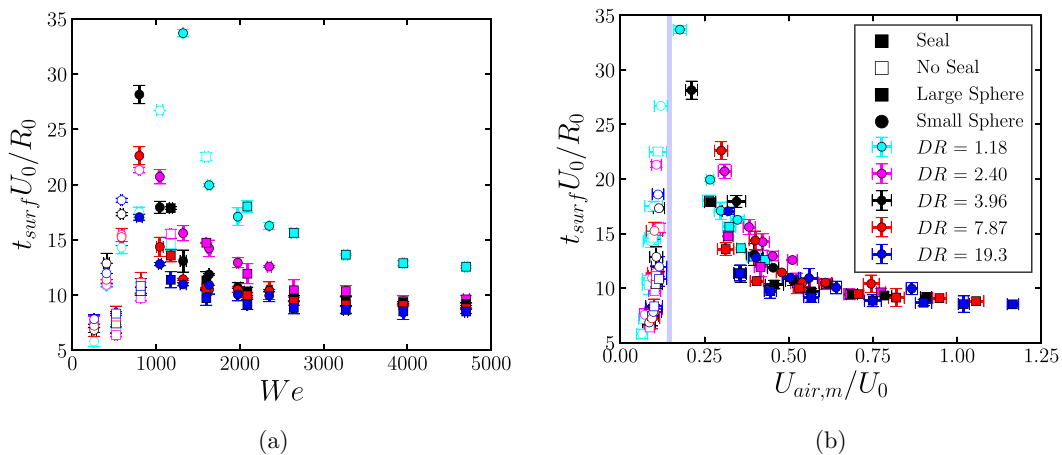


FIG. 6. Dimensionless surface-seal time as a function of (a) We defined based on sphere impact velocity, $We = \frac{\rho U_0^2 R_0}{\sigma}$, (b) ratio of air entrainment velocity to the sphere impact velocity, $U_{air,m}/U_0$. The predicted critical air entrainment velocity ratio from the mathematical model [Eq. (21)] is $U_{air,m}/U_0 \approx 0.146$ with an uncertainty of $\approx \pm 0.005$ (calculated based on the rounded rim radius, a , uncertainty).

cavities typically undergo a rapid increase in pressure difference (across the splash curtain) before dome closure, while a more gradual increase in pressure difference leads to a cavity without surface seal. Therefore, we can hypothesize that the closure dynamics of the splash is dominated by the pressure difference across it generated by cavity expansion and airflow into the cavity. Thus, to find the proper scaling for the dimensionless surface-seal time, we only use pressure difference force to rewrite the equation of motion in the radial direction, \hat{r} , for the whole splash curtain

$$m \frac{d^2 \vec{R}(t)}{dt^2} = \frac{1}{2} \rho A U_{air,m}^2, \quad (14)$$

where m is the splash curtain mass and can be approximated as, $\rho A w$. Here, A and w are the splash curtain surface area and thickness, respectively. Also, $U_{air,m}$ is the temporal mean of the air velocity averaged over the period of the sphere's impact to surface closure. Substitution leads to

$$\frac{d^2 \vec{R}(t)}{dt^2} = \frac{1}{2w} U_{air,m}^2 \approx \text{const.} \quad (15)$$

Solving Eq. (15) for $\vec{R}(t)$ yields

$$\vec{R}(t) = R_0 - \frac{1}{4w} U_{air,m}^2 t^2. \quad (16)$$

At the instant of the surface seal, $\vec{R}(t = t_{surf}) = 0$, and we find $t_{surf} = \sqrt{4wR_0}/U_{air,m}$. Assuming that the curtain thickness is a linear function of the sphere radius [15], $w \propto R_0$, surface-seal time is deduced to be proportional to

$$t_{surf} \propto \frac{R_0}{U_{air,m}}. \quad (17)$$

This suggests that the proper scaling for dimensionless surface-seal time is defined based on the velocity of airflow into the cavity

$$\frac{t_{surf} U_0}{R_0} \propto \frac{1}{\frac{U_{air,m}}{U_0}}. \quad (18)$$

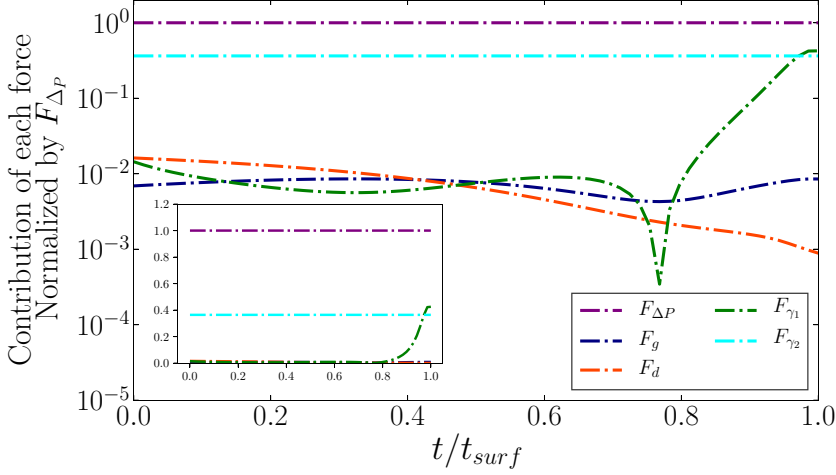


FIG. 7. The mean contribution of each force in Eq. (12) normalized by the magnitude of $F_{\Delta P}$.

Thus, we plot the dimensionless surface-seal time as a function of air entrainment velocity to the impact velocity ratio in Fig. 6(b). This plot indicates that this scaling enables us to obtain one single transition air velocity ratio from no surface-seal regime to surface-seal regime for all the spheres with different density and size. According to the experimental observations, the critical air velocity ratio for the occurrence of the surface seal is between 0.14 and 0.17.

Now, the model is used to find the critical airflow velocity beyond which the surface seal occurs. By revisiting Eq. (12) and conducting a scaling analysis, this equation is reduced to

$$\frac{d^2 R(t)}{dt^2} = -\frac{1}{\pi a} U_{\text{air},m}^2 + \frac{2\gamma}{\rho \pi a^2}. \quad (19)$$

To derive Eq. (19) from Eq. (12), we ignored the gravity, centrifugal acceleration, and air drag forces. Since the air density is low, $Fr \gg 1$, and the mass of the rim is small, these forces should only exert a minor influence. To confirm that these forces are safely neglected, it would therefore be essential to compare the magnitude of the different contributions in Eq. (12). Hence, we compare the contribution of each force ($\sqrt{\vec{F}_r + \vec{F}_z}$) in Eq. (12).

Thus, Fig. 7 indicates it is safe to ignore the centrifugal, gravity, and drag forces to derive Eq. (19). It also demonstrates that a model developed to explain the dynamics of the splash curtain must account for both pressure difference and surface tension forces and the surface seal predominantly is governed by pressure difference force. Assuming that the pressure differential is negligible explains why the model by Ref. [15] does not predict the surface-seal time accurately when compared with our experimental results (See Appendix 2).

We solve Eq. (19) for $R(t)$ and set it equal to zero to find the surface-seal time

$$t_{\text{surf}} = \sqrt{\frac{R_0}{\left[\frac{R_0}{\pi a U_0^2} U_{\text{air},m}^2 - \frac{2\gamma R_0}{\rho \pi a^2 U_0^2} \right]}}. \quad (20)$$

This equation has a real solution when the denominator is greater than zero, and, in that case, the occurrence of the surface seal is assured. Therefore, the singularity of Eq. (20) corresponds to the transition from no seal regime to surface-seal regime, and it is formulated as

$$\frac{U_{\text{air},m}^2}{U_0^2} = \frac{2\gamma}{\rho a U_0^2} = \frac{2}{We_c} \frac{R_0}{a}, \quad (21)$$

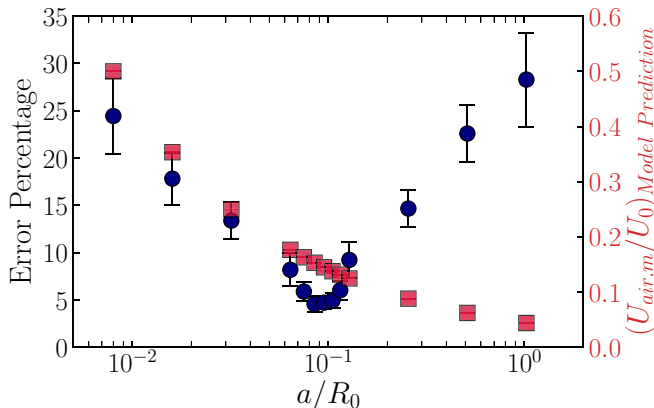


FIG. 8. Model outputs sensitivity to the rim radius. The error percentage for each drop is calculated as: $\frac{\sum_{t=0}^{t_{\text{surf}}} (\text{Observed rim's location} - \text{Predicted rim's location})}{\text{Observed rim's location}} \times 100$. The markers correspond to the mean value (of all the drops) and the error bars show the standard deviation. Circle markers represent the error percentage and the squares correspond to the predicted criterion for the occurrence of surface seal.

where We_c is the critical Weber number for the occurrence of the surface seal, defined based on sphere impact velocity. Experiments show that most of the cases with We greater than 1000 are associated with surface seal. Using experimental estimation for rounded rim radius, $a \approx 0.095R_0$ ($a/R_0 \approx 0.095 \pm 0.007$), and choosing $We_c \approx 1000$, we can establish $U_{\text{air},m}/U_0 \approx 0.146$ as a criterion for the occurrence of surface seal [Eq. (21)], which is consistent with experiments [see Fig. 6(b)].

Rim radius, a , is a crucial input parameter for the model. Although we propagated the uncertainty in the measurement of the rim radius through the model to find the uncertainty on the predicted $U_{\text{air},m}/U_0$ threshold by the model ($U_{\text{air},m}/U_0 = 0.146 \pm 0.005$), it is also essential to study how much an error in a affects the predicted trajectory of the curtain's rim. Figure 8 shows the sensitivity of the model outputs (trajectory of the rim and prediction of transition threshold from no seal regime to surface-seal regime) to the selection of rim radius.

The results indicate that with a 50% error in the determination of rim's radius, less than 10% error is observed between the model's predictions and the observations.

Even though we focused on the dynamics of the splash curtain of the water-entering spheres, the model can be generalized to predict the splash curtain of projectiles with various geometries.

VI. CONCLUSION

This work presented detailed analysis and physical understanding of why a splash does not always seal, supported by a developed theory and experimental observations. Contrary to current understanding, our observation showed projectile impact velocity is not the governing parameter determining the occurrence of surface seal, and projectile density and size are also determinant factors in this phenomenon. We developed a physical model to predict the trajectory of the splash curtain. This model enabled us to discover the existence of a critical dimensionless number that predicts the occurrence of surface seal and revealed that the velocity of the airflow rushing into the cavity is the determinant factor in the surface seal. Therefore, we determined the critical airflow velocity ratio beyond which the surface seal occurs in the water entry of hydrophobic spheres.

ACKNOWLEDGMENT

This work was supported by the NSF under Grant No. CBET-1336038.

APPENDIX

1. Methods: Splash curtain imaging

Finding the experimental trajectory of the splash curtain from a typical shadowgraph video similar to Ref. [19] is difficult and can impose high error in the rounded rim determination. Instead, we developed a variation of shadowgraph imaging by capturing the shadow of the splash curtain on a transparent high-quality paper. To do so, we used a point light source to make the shadow of the splash on the transparent paper (using the point light source is crucial in order to prevent the creation of any penumbra and antumbra in the shadow, i.e., creation of sharp edge images), and focused the camera on the transparent paper instead of real splash curtain [35]. These images are then converted to binary images, enabling us to determine the rounded rim location of the splash curtain in a robust way: we obtained the splash curtain boundary profile and found the first inflection point from the bottom of it as the location of rounded rim in each frame (Fig. 9).

We also found the rounded rim radius from the obtained curtain profile. This operation was performed for every frame of every case which resulted in a time history of rounded rim radius for each case. We averaged it over time for each individual drop and then calculated the mean and standard deviation for all the drops (Fig. 9).

2. A comparison between our experimental observations and the predictions by Aristoff and Bush model

We use the obtained experimental parameters in the current study (impact velocity) into the Aristoff and Bush model [15] and compare the dimensionless surface seal predicted by this model with our experimental data.

Figure 10 shows the deviation of predictions by the Aristoff and Bush model from the experimental data. To produce this plot, we employ the model of Ref. [15] with $\theta_c = 170^\circ$ and $\delta_0 = 0.02$ cm. Note that the predictions of the model of Ref. [15] are sensitive to both initial film thickness, δ_0 , and “cone angle,” and both of these are not measurable quantities. Cone angle, θ_c , in Ref. [15] is defined as: “the angle that the cavity makes as it leaves the sphere with respect to the vertical tangent it is approximately constant as a function of depth and body speed for a given surface material.” The maximum deviation of the predicted dimensionless surface-seal time from the experiment is 278% for Ref. [15] and 5.6% for the model presented in this study.

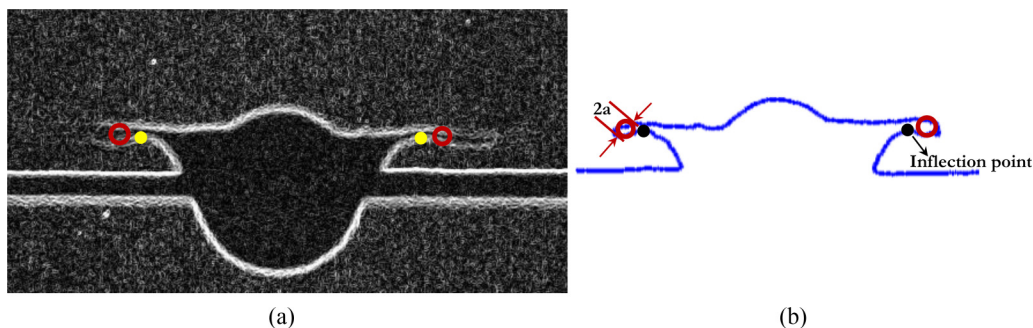


FIG. 9. Locating splash curtain rounded rim by finding the splash curtain boundary profile from the shadow videos [35]: (a) Identified boundary profile of the splash curtain from binarized image. (b) Extracted boundary profile. The deflection point and identified rounded rim are shown by solid and open marker, respectively. The location of the rounded rim center is defined as the first inflection point (from the bottom) in the splash curtain boundary profile. The rounded rim radius is approximated as the radius of the closest identified circular object (in the splash curtain boundary profile) to the inflection point in a registered image around the inflection point.

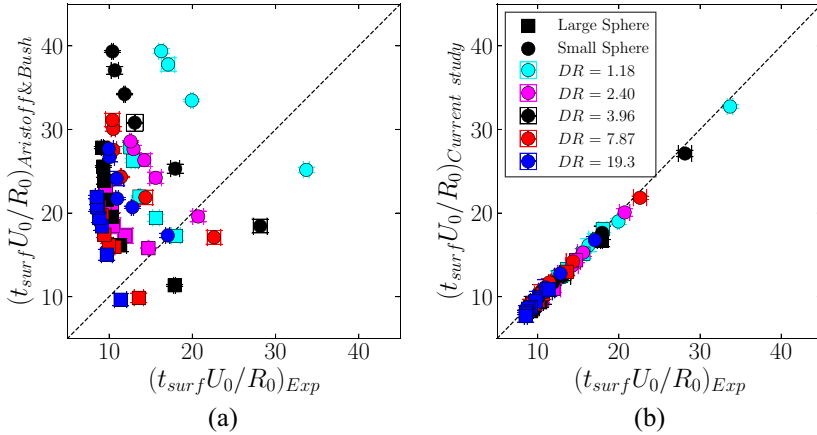


FIG. 10. Prediction for dimensionless surface-seal time vs experimental data: (a) Aristoff and Bush model [15], (b) the proposed model in the current study.

Regarding the shape of the splash curtain, because our model predicts the trajectory of the splash curtain's rim, a direct comparison with the model prediction by Ref. [15] is not possible. However, a qualitative comparison with Ref. [15] shows deviation in the splash curtain prediction.

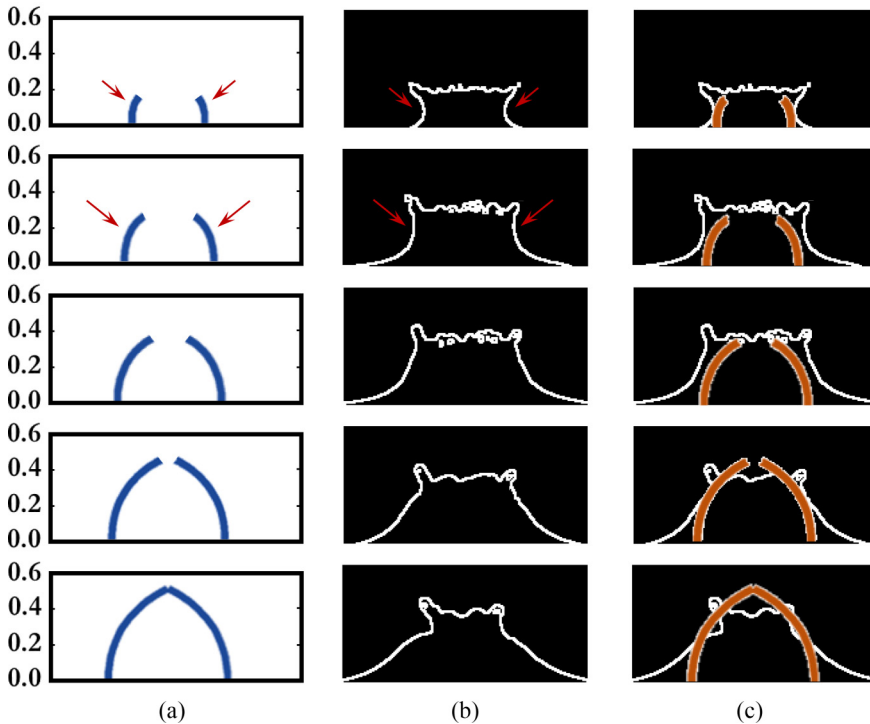


FIG. 11. Comparison of the shape of splash curtain predicted by Aristoff and Bush model and their experimental observations: (a) model prediction by Ref. [15], (b) splash boundary of experimental observation by Ref. [15] detected by our imaging-processing scheme, and (c) superimposition of experimental observation and model prediction. Red arrows show the deviation of splash curvature in model prediction from the experiment.

The experimental observations show that the splash curtain ejects upwards and outwards, while in contrast, the predicted shape by Ref. [15] is an upwards and inwards splash curtain. To show this deviation, we performed image processing on the experimental images of Fig. 18 in Ref. [15] and are superimposed with their model predictions in Fig. 11, below.

Figure 11 indicates that the model by Ref. [15] does not capture the curvature of the splash curtain, and how significantly this model prediction deviates from the experimental observation.

-
- [1] R. Bergmann, D. van der Meer, M. Stijnman, M. Sandtke, A. Prosperetti, and D. Lohse, Giant Bubble Pinch-Off, *Phys. Rev. Lett.* **96**, 154505 (2006).
 - [2] V. Duclaux, F. Caillé, C. Duez, C. Ybert, L. Bocquet, and C. Clanet, Dynamics of transient cavities, *J. Fluid Mech.* **591**, 1 (2007).
 - [3] S. Gekle, J. M. Gordillo, D. van der Meer, and D. Lohse, High-Speed Jet Formation after Solid Object Impact, *Phys. Rev. Lett.* **102**, 034502 (2009).
 - [4] S. Gekle, J. H. Snoeijer, D. Lohse, and D. van der Meer, Approach to universality in axisymmetric bubble pinch-off, *Phys. Rev. E* **80**, 036305 (2009).
 - [5] J.-F. Louf, B. Chang, J. Eshraghi, A. Mituniewicz, P. P. Vlachos, and S. Jung, Cavity ripple dynamics after pinch-off, *J. Fluid Mech.* **850**, 611 (2018).
 - [6] T. T. Truscott, B. P. Epps, and A. H. Techet, Unsteady forces on spheres during free surface water entry, *J. Fluid Mech.* **704**, 173 (2012).
 - [7] T. T. Truscott and A. H. Techet, Water entry of spinning spheres, *J. Fluid Mech.* **625**, 135 (2009).
 - [8] J. M. Aristoff, T. T. Truscott, A. H. Techet, and J. W. M. Bush, The water entry of decelerating spheres, *Phys. Fluids* **22**, 032102 (2010).
 - [9] A. M. Worthington, *A Study of Splashes* (Longmans, Green, and Company, London, 1908).
 - [10] D. Gilbarg and R. A. Anderson, Influence of atmospheric pressure on the phenomena accompanying the entry of spheres into water, *J. Appl. Phys.* **19**, 127 (1948).
 - [11] Y. L. Yakimov, Effect of the atmosphere with the fall of bodies into water, *Fluid Dyn.* **8**, 679 (1973).
 - [12] H. I. Abelson, Pressure measurements in the water-entry cavity, *J. Fluid Mech.* **44**, 129 (1970).
 - [13] M. Lee, R. G. Longoria, and D. E. Wilson, Cavity dynamics in high-speed water entry, *Phys. Fluids* **9**, 540, (1997).
 - [14] J. O. Marston, T. T. Truscott, N. B. Speirs, M. M. Mansoor, and S. T. Thoroddsen, Crown sealing and buckling instability during water entry of spheres, *J. Fluid Mech.* **794**, 506 (2016).
 - [15] J. M. Aristoff and J. W. M. Bush, Water entry of small hydrophobic spheres, *J. Fluid Mech.* **619**, 45 (2009).
 - [16] A. May, Effect of surface condition of a sphere on its water-entry cavity, *J. Appl. Phys.* **22**, 1219 (1951).
 - [17] E. G. Richardson, The impact of a solid on a liquid surface, *Proc. Phys. Soc.* **61**, 352 (1948).
 - [18] G. Birkhoff and E. H. Zarantonello, *Jets, Wakes and Cavities* (Academic Press, New York, 1957).
 - [19] See Supplemental Material at <http://link.aps.org/supplemental/10.1103/PhysRevFluids.5.104001>, Movie S1(a), for a video of splash curtain evolution.
 - [20] See Supplemental Material at <http://link.aps.org/supplemental/10.1103/PhysRevFluids.5.104001>, Movie S1(b), for a video of cavity evolution.
 - [21] G. Birkhoff and R. Isaacs, Transient cavities in air-water entry, Navord Report No. 1490 (1951).
 - [22] M. M. Mansoor, J. O. Marston, I. U. Vakarelski, and S. T. Thoroddsen, Water entry without surface seal: Extended cavity formation, *J. Fluid Mech.* **743**, 295 (2014).
 - [23] A. May, Vertical entry of missiles into water, *J. Appl. Phys.* **23**, 1362 (1952).
 - [24] J. W. Glasheen and T. A. McMahon, Vertical water entry of disks at low Froude numbers, *Phys. Fluids* **8**, 2078 (1996).
 - [25] See Supplemental Material at <http://link.aps.org/supplemental/10.1103/PhysRevFluids.5.104001>, Fig. S1, for cavity characteristics plots.

- [26] A. L. Yarin, Drop impact dynamics: Splashing, spreading, receding, bouncing . . . , *Annu. Rev. Fluid Mech.* **38**, 159 (2006).
- [27] R. Clift, J. R. Grace, and M. E. Weber, *Bubbles, Drops, and Particles* (Academic Press, New York 1978).
- [28] S. Gart, B. Chang, B. Slama, R. Goodnight, S. H. Um, and S. Jung, Dynamics of squeezing fluids: Clapping wet hands, *Phys. Rev. E* **88**, 023007 (2013).
- [29] L. Vincent, T. Xiao, D. Yohann, S. Jung, and E. Kanso, Dynamics of water entry, *J. Fluid Mech.* **846**, 508 (2018).
- [30] W. S. Cleveland, Robust locally weighted regression and smoothing scatterplots, *J. Am. Stat. Assoc.* **74**, 829 (1979).
- [31] A. Etebari and P. P. Vlachos, Improvements on the accuracy of derivative estimation from DPIV velocity measurements, *Exp. Fluids* **39**, 1040 (2005).
- [32] See Supplemental Material at <http://link.aps.org/supplemental/10.1103/PhysRevFluids.5.104001>, Movie S2, for splash curtain rounded rim trajectory: Experimental observation vs model prediction.
- [33] See Supplemental Material at <http://link.aps.org/supplemental/10.1103/PhysRevFluids.5.104001>, Fig. S2, for the effects of sphere density and impact velocity on the rim trajectory.
- [34] See Supplemental Material at <http://link.aps.org/supplemental/10.1103/PhysRevFluids.5.104001>, Movie S3, for We scaling failure to identify a critical We for transition from no surface-seal regime to surface-seal regime for all the spheres with different density and size.
- [35] See Supplemental Material at <http://link.aps.org/supplemental/10.1103/PhysRevFluids.5.104001>, Movie S4, for splash curtain imaging.